Carbon-coated FePO4 nanoparticles as stable cathode for Na-ion batteries: A promising full cell with a Na15Pb4 anode

Bidhan Pandit, Bernard Fraisse, Lorenzo Stievano, Laure Monconduit, Moulay Tahar Sougrati

Version of Record: https://www.sciencedirect.com/science/article/pii/S0013468622001694
Manuscript_e0c7d18b73fbb5cb0bf7584b09b07728

Carbon-coated $FePO_4$ nanoparticles as stable cathode for Na-ion batteries: A promising full cell with a $Na_{15}Pb_4$ anode

Bidhan Pandit[1], Bernard Fraisse[1], Lorenzo Stievano[1,2], Laure Monconduit[1,2], Moulay Tahar Sougrati[*,1,2]

1. *ICGM, Univ. Montpellier, CNRS, ENSCM, Montpellier, France*
2. *RS2E, CNRS, Amiens, France*

*__Corresponding Author__: Moulay-Tahar.Sougrati@umontpellier.fr

Abstract

The cheap and non-toxic $FePO_4$, which can be recovered from spent LFP batteries, provides a reversible capacity of 103 mAh/g in coin cells, corresponding to 76% of theoretical capacity, with very good rate capability and stability. The study of the electrochemical mechanism during sodiation carried out by *in situ* X-ray diffraction (XRD) reveals a pure biphasic transition during Na^+ (de)insertion. The chemical diffusion coefficient (D_{Na}) determined from galvanostatic intermittent titration technique and electrochemical impedance spectroscopy varies in the range 10^{-16}-10^{-10} cm^2/s at room temperature depending on the degree of sodiation. As a proof of concept, a full cell fabricated using a carbon-coated C@$FePO_4$ cathode and a $Na_{15}Pb_4$ anode obtained by electrochemical sodiation of recyclable Pb, maintained 76% of the initial capacity over 100 cycles at constant C/10 rate. This outstanding electrochemical performance, based on the combination of the low-cost C@$FePO_4$ cathode with a recyclable lead-based anode, makes this new technology a promising real-world alternative for future commercial Na-ion systems.

Keywords: Sodium-ion batteries, Cathode materials, $FePO_4$, GITT, Full cells

1. Introduction

Sodium-ion batteries (SIBs) have been recently proposed as a complement to lithium-ion batteries (LIBs) for large-scale energy storage application, because of their low cost, excellent performance, and the wide availability of sodium [1–5]. Owing to the much larger size and atomic weight of Na^+ (1.06 Å, 22.99 g/mol) compared with Li^+ (0.76 Å, 6.94 g/mol), the identification of a suitable intercalation electrode material that can ensure reversible (de)intercalation of sodium ions without a significant volume change and/or structural degradation has long been pursued [6]. To realise a working SIB technology, a crucial issue is to realize relevant Na^+ host materials for both negative and positive electrodes [7–10]. Until nowadays, a variety of materials, such as transition metal oxides [11–15], phosphates [16–18], Prussian blue analogues [19,20], carbodiimides [21,22], metal alloys [23–26] and hard carbons [27,28], have been proposed as anode/cathode materials. Many of these materials exhibit good reversible capacity and cycling stability, demonstrating the practical feasibility of SIBs.

In particular, transition metal phosphates with olivine crystal structure have gained a noticeable attention as SIB cathodes due to their worthy charge-discharge kinetics, high operation voltage, and safety properties [29–33]. Nevertheless, Ni, V, and most of all Co phosphates are not desirable as electrode materials for large-scale energy storage given their rareness/cost and their ecological/environmental impact. Iron, on the contrary, is abundant, widespread and much cheaper. Indeed, Fe-based cathode materials have motivated great attention for the development of safe and low-cost SIBs [34], and among them, iron phosphates have shown particularly attractive properties [35].

Differently from $LiFePO_4$ (LFP), an excellent commercial cathode for LIBs with well-known properties [16], olivine (triphylite) $NaFePO_4$ (NFP) is a metastable polymorph, the thermodynamic stable form crystallising with the maricite structure [36]. As a consequence, the direct synthesis of olivine NFP is practically impossible, and a common way to obtain it is by sodiating previously delithiated LFP [37]. In spite of the similar crystal structure,

thermodynamics and kinetics for Na^+ (de)insertion in olivine NFP are slightly different from the corresponding (de)lithiation process in LFP [38,39]. The low electronic conductivity of NFP, which has a strong impact on its cycling performance, can be improved by carbon coating, leading to a strong improvement of the electronic conductivity. However, the coating process must be applied to the pristine LFP before its delithiation to avoid a possible reduction of the Fe^{3+} contained in $FePO_4$. So, starting from commercial carbon-coated LFP can be a good option for obtaining $FePO_4$/C by a one-step chemical delithiation. Alternative strategies to improve the electronic conductivity include doping and composite engineering by embedding the $FePO_4$ particles into a conductive matrix. Fan *et al.* a simple method to directly grow $FePO_4$ nanoparticles on graphene nanosheets with a reversible capacity of 92 mAh/g at 0.2 C with good rate capability [40]. Liu *et al.* showed that adequately mixing $FePO_4$ nanoparticles with single-walled carbon nanotubes leads to enhanced electrochemical performance and improved cycling stability [41]. Similarly, Fang *et al.* demonstrated that mesoporous $FePO_4$ nanospheres with conductive carbon exhibit a higher discharge capacity and better cycle stability [42].

In this work, a carbon-coated $FePO_4$@C (FP@C) composite obtained by chemical delithiation of a commercial carbon-coated LFP@C precursor was evaluated as cathode material for SIBs. The optimised contact between the electrochemically active $FePO_4$ particle and the outer conductive carbon coating acting as an effective electron transport pathway provides improved performance in comparison with the simple mixture of the two separate components, especially at high current rates. Such a promising cathode was assembled in full cell vs. a lead-based anode, $Na_{15}Pb_4$, previously obtained by electrochemical sodiation of Pb metal. Indeed, lead is a promising alloying negative electrode material which has recently shown excellent performance in SIBs with gravimetric and volumetric capacities higher than traditional carbonaceous anodes [43,44]. Moreover, due to its widespread application in lead-acid systems, the recovery of Pb from spent batteries is a perfectly established technology, with a

recycling rate exceeding 99%. Such a combination therefore represents an original and viable battery technology featuring long cycle life, excellent energy/power densities and safety.

2. Experimental details

2.1 Carbon-coated FP synthesis

The core-shell FP@C composite was prepared by the chemical oxidation process of a commercial carbon-coated lithium iron (II) phosphate ($LiFePO_4$@C, Triphylite) by taking inspiration from the method of Armand and co-workers [45]. The wet chemical oxidation of commercial C@LFP was achieved in excess of $(NH_4)S_2O_8$ (1.2 mole of $(NH_4)S_2O_8$ per mole of LFP) starting from an aqueous suspension of 1 g of LFP in 50 ml of deionised water via the following reaction:

$$2LiFePO_4 + (NH_4)_2S_2O_8 \rightarrow 2FePO_4 + (NH_4)_2SO_4 + Li_2SO_4 \qquad (1)$$

The black solid was then filtered, washed with distilled water and ethanol for several times, and dried in air at 60°C for overnight.

It is worth noting that reaction (1) allows the recovery of Li^+ as lithium sulphate. Therefore, this method could be very efficient in the recycling of spent LFP batteries (not used here) to convert them to FP to be used in Na-ion batteries and hence starting from waste materials instead of using fresh LFP.

2.2 Material characterization

X-ray diffraction (XRD) patterns were measured on a D8 Advance Bruker instrument using the monochromatic CuKα radiation (λ = 1.5406 Å). Full pattern matching refinement was carried out with the FullProf program using the pseudo-Voigt profile function. Raman studies were performed with a Horiba LabRAM HR, with a 633 nm laser excitation beam. X-ray photoelectron spectroscopy (XPS) analysis was carried out on a ESCALAB 250 (ThermoElectron) spectrometer with Al Kα excitation source (1486.6 eV). Morphology and composition of the materials were characterized by using a scanning electron microscope

(Hitachi S-4800) and a high-resolution transmission electron microscope (TECNAI G2 20 Twin, FEI) equipped with an Energy Dispersive X-ray (EDX) detector. ^{57}Fe Mössbauer spectra were measured at room temperature (293 K) with a ^{57}Co:Rh source and a Kr gas proportional counter. The spectrometer was operated with a triangular velocity waveform, and the spectra were fitted with superpositions of appropriate sets of Lorentzian lines using the PC-MOS computer program [46]. Thermogravimetric analysis (TGA) was performed under airflow in the temperature range of 20–800 °C using a Netzsch STA-449 F1 Jupiter analyser.

2.3 Electrochemical characterization

The electrochemical properties of the FP@C composite were studied in standard coin cells assembled in an argon-filled glove box. Electrode formulation was made using a mixture of carbon black and vapour-grown carbon fibers (VGCF-H) as conductive additives, and Poly(vinylidene fluoride) (PVdF) as the binder, suspended in 1-Methyl-2-pyrrolidinone (NMP, anhydrous, 99.5%). A slurry containing the active material (70%), the binder (12%) and the conductive additive (18%) was homogeneously mixed in a planetary ball-milling for 1 h, tape casted on an aluminium foil (18 µm), dried at room temperature for 12 h and finally at 80 °C under vacuum overnight. The final mass loading of active material on the electrode can be varied between 2 and 10 mg/cm^2 by slightly modifying the viscosity of the initial slurry.

Electrochemical tests in half-cell were performed against a Na (Sigma-Aldrich, purity >99.9%) counter-electrode, using an electrolyte of 1 M $NaPF_6$ dissolved in diglyme. Whatman glass-fiber was used as separator. All tests were carried out at room temperature (25 °C) in the galvanostatic mode between 1.5 and 4.0 V vs Na^+/Na at C/n rate (corresponding to the reaction of 1 mole of Na per mole of FP in n hours).

Electrochemical impedance spectroscopy (EIS) measurements were performed using three-electrode Swagelok-type cells. The FP@C electrode was assembled as the working electrode, while two separate foils of Na metal were used as counter and reference electrode.

Galvanostatic intermittent titration technique (GITT) measurements were performed in a 3-electrode Swagelok cell: the cell was charged for 1h at a current rate of C/10, followed by open circuit relaxation up to the condition dv/dt=0.1 mV/h. The evolution of the quasi-equilibrium potential vs. capacity in Na_xFePO_4 obtained from the GITT results is shown in Figure S4.

Finally, full cells were built with FP@C as cathode material and $Na_{15}Pb_4$ as anode. $Na_{15}Pb_4$ electrodes were obtained by electrochemical sodiation of Pb electrode in half-cells vs. Na metal; qs described in detail in ref. [47]: a slurry containing 98% Pb powder (Sigma–Aldrich, purity 99.95%, ~325 mesh), 1 % mixture of carbon black and vapor ground carbon fibers (VGCF-H) and 1 %Poly(vinylidene fluoride) (PVdF, Solef 5130, Solvay) in 1-Methyl-2-pyrrolidinone (NMP, anhydrous, 99.5% Sigma–Aldrich) was homogeneously mixed by a planetary ball-milling for 1 h, tape casted on a 150 μm thick copper foil, dried at room temperature for 12 h and finally at 120 °C *in vacuo* overnight. The so-obtained Pb electrodes were then directly sodiated in coin cells against a pure Na (Aldrich) counter-electrode using a 1 M $NaPF_6$/diglyme electrolyte. The electrode was then unmounted from the coin cell, rinsed twice in dyglime and dried *in vacuo* at room temperature before use. The modification of the viscosity of the initial slurry allows controlling the mass loading of anode active material, which can be varied between 1 and 10 mg/cm^2. The m_+/m_- (positive/negative) mass ratio was chosen at 5:1, based on the practical reversible capacity of the two electrodes, which is about 100 and 480 mAh/g at C/10 for $FePO_4$ and $Na_{15}Pb_4$, respectively (*vide infra*). For all full cell experiments, the C/n rate corresponds to the reaction of 1 mole of Na per mole of $Na_{15}Pb_4$ in n hours.

In situ XRD measurements were performed using a specifically designed *in situ* cell with an aluminium collector placed on beryllium window [48]. The *in situ* XRD cell was placed in an X'Pert Pro diffractometer with the Co K_α radiation. The cell was cycled at a low rate of C/30, and the interval between two successive X-ray patterns corresponds to 0.03 inserted or de-inserted Na^+.

3. Results and discussion

3.1 Structural and morphological analysis of FP@C

The X-ray diffraction pattern and the Raman spectrum of sample FP@C prepared by chemical delithiation of LFP@C are shown in Figures 1 and S1. XRD shows the presence of pure orthorhombic heterosite $FePO_4$ (space group Pnma) confirming the efficiency of the chemical delithiation. The refined cell parameters (a = 9.8184(2) Å, b = 5.7920(1) Å, c = 4.7835(1) Å are in good agreement with previous results [30,49]. As already shown in previous studies [50,51], the stretching modes of the PO_4^{3-} anion visible in the Raman spectrum as narrow bands above 900 cm^{-1} are diagnostic of the (de)lithiation state of $LiFePO_4$. The observed bands at 908, 959, 1068, and 1126 cm^{-1} thus confirm the presence of $FePO_4$. The most intense peaks in the Raman spectrum in the 1200-1600 cm^{-1} range, however, are the typical D and G bands of carbon, generally attributed to disorder-induced modes related to structural defects in carbon and to the first-order scattering of the E 2g phonon of C sp^2 atoms, respectively [52]. The D-to-G band intensity ratio ($R = I_D/I_G$) can be used to evaluate the graphitization degree of carbon materials, and in this specific case the R value is 1.09, indicating a rather disordered carbon structure.

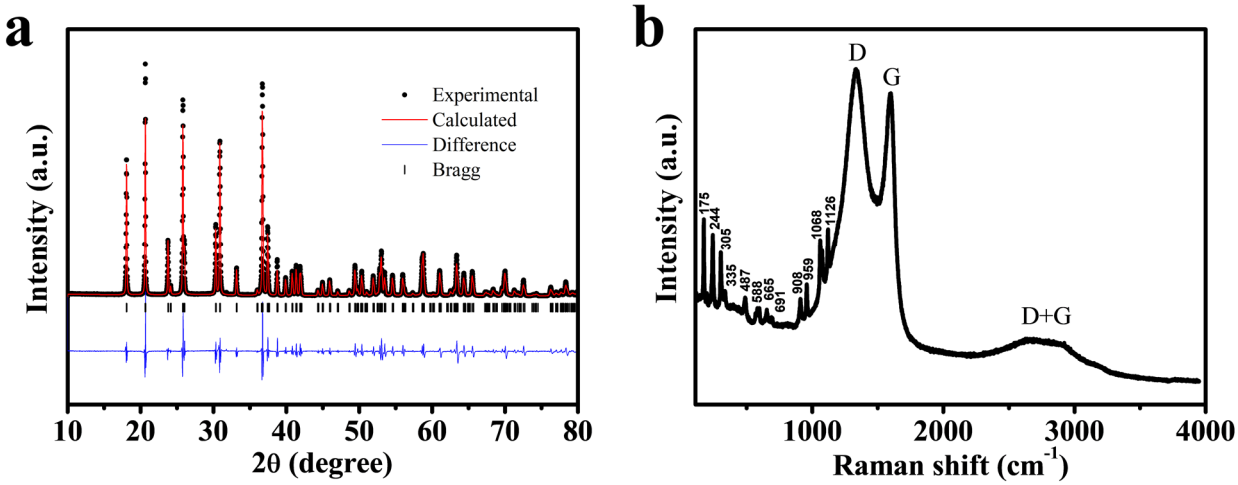

Figure 1: (a) FP@C X-ray diffraction pattern (Cu K_α source) with Rietveld refinement and (b) Raman scattering spectrum (633 nm laser).

The XPS spectra of FP@C are shown in Figure 2. The peaks at 725.8, 712.1, and 715.1 eV in the Fe 2p spectrum confirm the presence of Fe(III), whereas no Fe(II) is detected, at least on the surface of powder grains [53]. The P 2p spectrum, on the other hand, clearly show a spin-orbit doublet with a dominant contribution at 133.3 eV, typical of the phosphate group of $FePO_4$ [54]. The O 1s spectrum shows the presence of two oxygen signals at 531.2 and 532.9 eV attributed to lattice oxygen and surface hydroxyls, respectively, while the C 1s spectrum shows a dominant peaks at 284.4 eV, typical of carbon black, and two minor peaks at 286 and 288.3 eV, attributed to surface C-O and carboxyl groups, respectively [53,54].

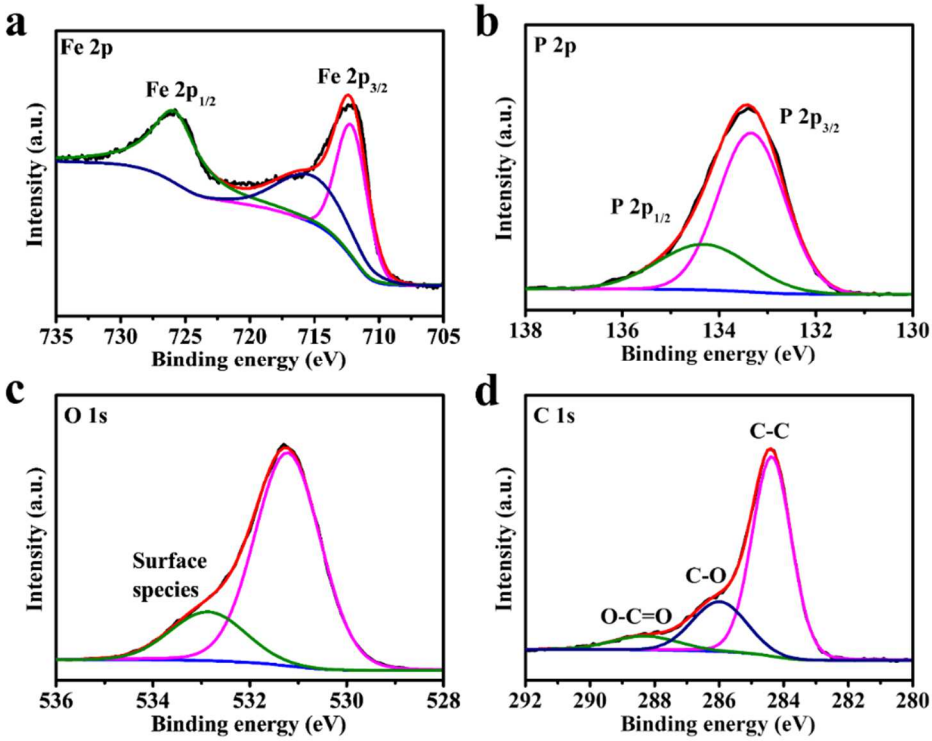

Figure 2: High-resolution XPS spectra of (a) Fe 2p, (b) P 2p, (c) O 1s, and (d) C 1s of the as-prepared FP@C.

The room temperature ^{57}Fe Mössbauer spectrum of FP@C shown in Figure 3 consists of a major quadrupole doublet with hyperfine parameters (Table 1) typical of the high-spin octahedral Fe(III) occupying the M2-site of heterosite. A minor component corresponding to about 13 % of the iron, with hyperfine parameters in the typical range of high-spin Fe(III) likely located in M1 antisite or surface defects of $FePO_4$ [55]. XPS and Mössbauer spectroscopy

together testify the complete oxidation of the Fe(II) in LFP to Fe(III) by chemical treatment in both bulk and surface of FP@C particles.

Table 1: Room temperature ^{57}Fe Mössbauer hyperfine parameters of FP@C.

Components	δ (mm/s)	Δ (mm/s)	Γ (mm/s)	Area (%)	Site
Comp1	0.43(1)	1.54(1)	0.24(2)	87(1)	Fe(III) in B-site of $FePO_4$
Comp2	0.41(1)	0.65(2)	0.45(3)	13(1)	Fe(III) in A-antisite or surface defects of $FePO_4$

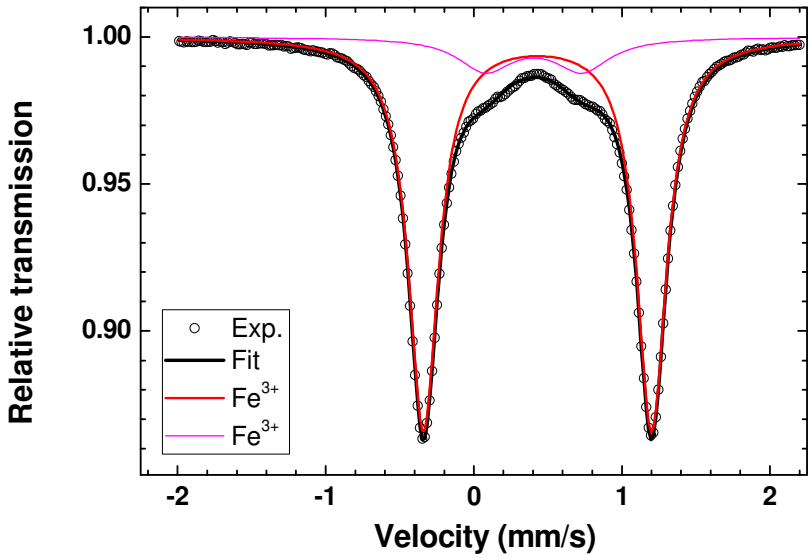

Figure 3: Room temperature ^{57}Fe Mössbauer spectrum of sample FP@C.

The carbon content of FP@C was determined by TGA in air flow (cf. Figure S2). Two mean sequential losses are observed around 100 °C and 500 °C, attributed to physisorbed water and carbon oxidation, respectively. The carbon content determined in this way is about 1.4 wt. %.

The SEM analysis of FP@C, shown in Figure 4, reveals that FP@C consists of quasi-spherical particles with sizes ranging from 50 to 300 nm resulting from the aggregation of primary $FePO_4$ nanoparticles. EDS analyses (cf. Figure S3 & Table S1) confirm the average composition of FP@C with an element ratio Fe : P : O = 1 : 1 : 4, as expected for $FePO_4$. The associated EDS elemental mapping (Figure 4c-h) shows the homogeneous distribution profiles of Fe, P, O and C over the surface for the composite.

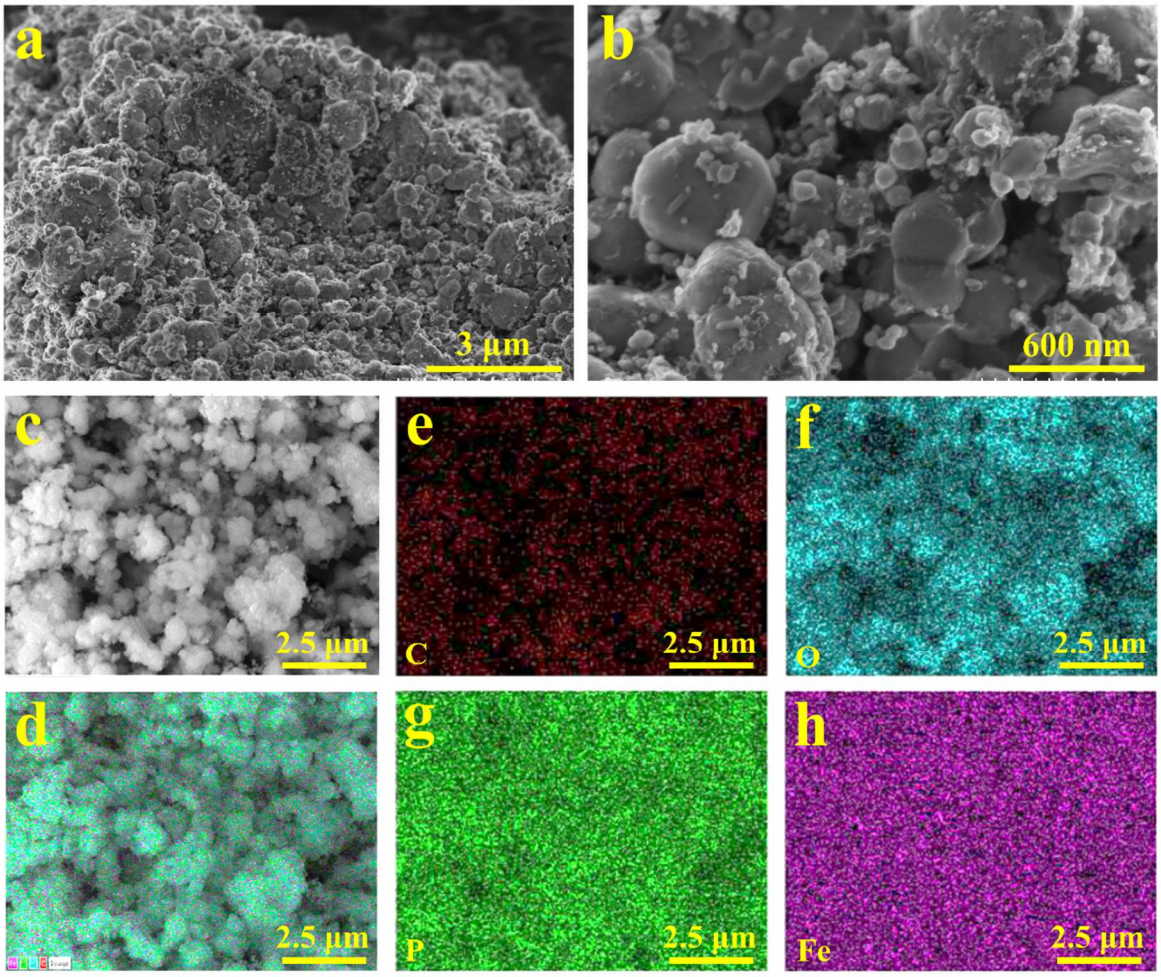

Figure 4: (a, b) SEM images of FP@C sample. (c-h) Corresponding EDS elemental mapping. (Elements are indicated in the left bottom corners)

3.2 Electrochemical performance

The performance of the FP@C composite as cathode material for SIBs was evaluated by galvanostatic cycling (Figure 5). A first activation cycle is performed at C/30, with a discharge capacity exceeding 130 mAh/g, conforming to 0.78 inserted Na^+, out of which only 0.61 can be recovered during the subsequent charge, corresponding to a reversible capacity of 103 mAh/g. This reversible capacity is significantly lower than the theoretical value of 178 mAh/g, which corresponds to the full (de)sodiation of $FePO_4$, but remains in line with those of other composites obtained using more complicated synthetic strategies [41,56]. It is interesting to notice that the shape of the first discharge profile is clearly different from the

following ones, underlining the importance of the activation step that occurs through a slightly different electrochemical path.

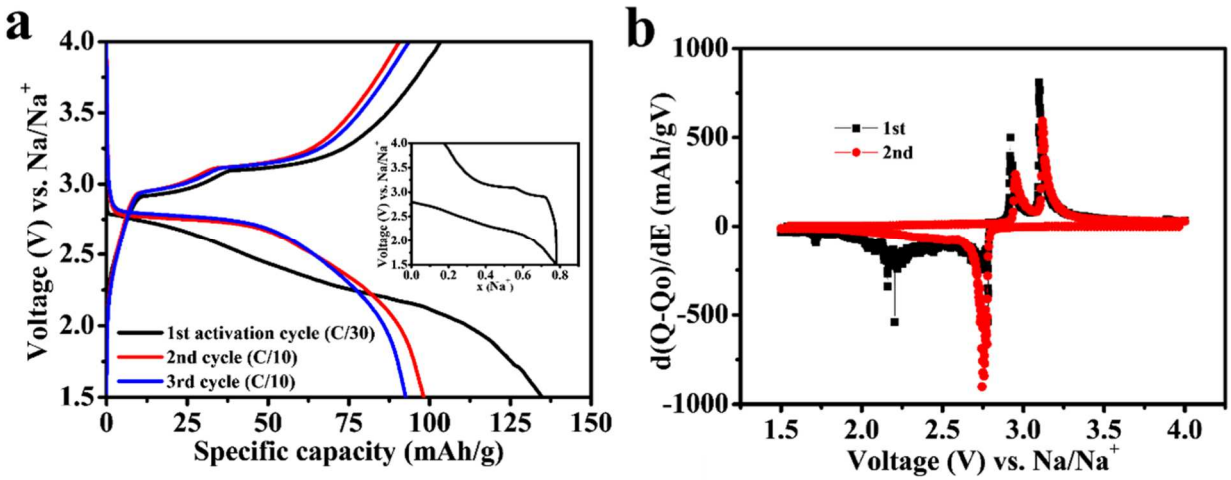

Figure 5: Galvanostatic charge/discharge curves (a) and corresponding derivative (b) of FP@C in half-cell vs. Na in 1 M $NaPF_6$/diglyme electrolyte at C/10 following a first activation cycle at C/30.

Cycle life and rate capability of FP@C are shown in Figure 6. The specific discharge capacities attain values of 100, 96, 85, 75 and 63 mAh/g at C/10, C/5 C/2, C and 2C, respectively. The capacity is fully recovered upon returning to C/10. After the first activation cycle, the associated coulombic efficiency remains very close to 100 % independently of the C-rate.

The long-term capacity retention of FP@C was tested at 2C rate (cf. Figure 6c). At this high rate, the capacity increases gradually during the first 80 cycles, and then remains virtually constant for the following 1000 cycles. The corresponding coulombic efficiency also remains very stable, close to 100% throughout the whole galvanostatic test. Such an increase in the capacity during the first cycles was already reported by Liu *et al.* in a recent study on FP/graphene composites, and tentatively attributed to the decrease of the FP particle size.[56] Indeed, as already mentioned above, the sodiation mechanism of FP is known to be different from the lithiation one, the former occurring with a lower rate constant, slower diffusion rate and higher activation energies.[57] In our case, we observe, during the first cycles, both a decrease of the polarisation with cycling, as well as a gradual amorphisation, at least during the first two cycles, as testified by the *operando* XRD study (vide infra). All these observations

go in the same direction, and indicate that the gradual amorphisation of the material with the number of sodiation/desodiation cycles induces an improvement of the diffusion of Na^+ in the FP channels. As a consequence, a decrease of the polarisation is observed which, given the slopy profile of the discharge curves, produces a slight increase in capacity and an increase of the number of cycles when the cycling rate is high. A similar trend, but for a smaller number of cycles, is observed also in the rate capability test shown in Figure 6a.

In addition to the intrinsically structural properties of FP, its excellent electrochemical performance most probably comes from the carbon coating, which improves the electronic percolation and provides an adequate electrode porosity for the electrolyte to access the electrode surface, thereby significantly alleviating the polarisation during the frequent discharge/charge steps, particularly at higher current densities.

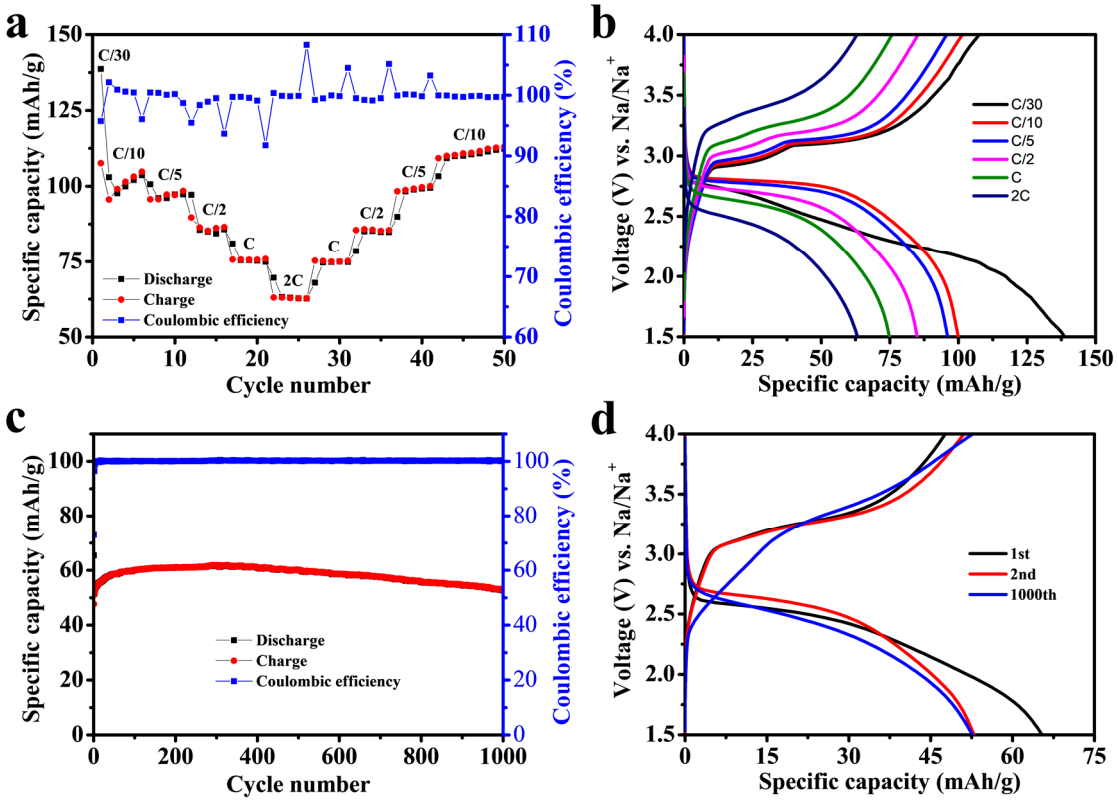

Figure 6: (a) Rate capability of FP@C electrode between C/10 and 2C. (b) Galvanostatic charge/discharge profiles at various current rates. (c) Cycling performance and Coulombic efficiency measured at 2C for 1000 cycles. (d) Galvanostatic charge/discharge profiles at various cycles.

The dynamics of Na^+ (de)insertion in $FePO_4$ can be studied by following their solid-state chemical diffusion coefficient (D_{Na}), a quantity that describe the property of ions transport under a concentration gradient. The Na^+ diffusion in the lattice of host is typically the important rate-determining step during charge/discharge of SIBs, and determining D_{Na} is therefore significant to recognize the fundamental kinetic property of electroactive material.

The D_{Na} values for FP@C estimated by both GITT and EIS (cf. Figures S4 and S5) in 3-electrode configuration range from 7.3×10^{-16} to 3.2×10^{-11} cm^2/s, and from 1.7×10^{-13} to 1.4×10^{-10} cm^2/s, respectively (cf. SI section for more details about the corresponding calculation methods). The values obtained by the two techniques, in good agreement between them, can be compared to previous literature report [58]. Tang *et al*. [59] reported the diffusion coefficient of $LiFePO_4$ in the range of 10^{-14}–10^{-18} cm^2/s.

3.3 Na^+ insertion/deinsertion mechanism

Operando XRD was used to investigate the insertion/extraction mechanism of Na^+ in FP@C (Figure 7). Before beginning the first discharge, all diffraction peaks can be indexed in the heterosite system. Upon discharging, a new set of peaks emerges, slowly replacing the gradually disappearing pattern of $FePO_4$ through a pseudo-biphasic mechanism. The mechanism is not purely biphasic, since, during the discharge, the pattern of $FePO_4$ is slightly modified with a gradual but steady shift of all reflections and a general increase of the linewidth before being totally consumed. The following charge, however, does not follow the same path, and at least one additional intermediate phase, which has a clear solid solution behaviour, appears along the desodiation. The formation of an intermediate phase with an average composition of $Na_{2/3}FePO_4$ had already been proposed by Galceran *et al.* [49], and its absence during the first sodiation can be clearly attributed to kinetic limitations, in agreement with previous literature [32]. So, the overall (de)sodiation can be expressed as the sequence of 2 bi-phasic processes, the intermediate phase having a solid solution existence domain. At the end of the charge process, the XRD pattern of $FePO_4$ is modified a little as compared to the pristine

$FePO_4$, with a slight shift of the reflections and a general increase of the linewidth. This indicates that pristine $FePO_4$ undergoes a partial irreversible modification/amorphisation during the first charge, most probably retaining some of the inserted Na^+ and thus named $Na_{0+\delta}FePO_4$. During the second discharge, the process also occurs via the formation of the $Na_{2/3}FePO_4$ intermediate, indicating that the kinetic limitations are lifted in the first sodiation process with the formation of the modified/amorphised $Na_{0+\delta}FePO_4$. (cf. Figure S6).

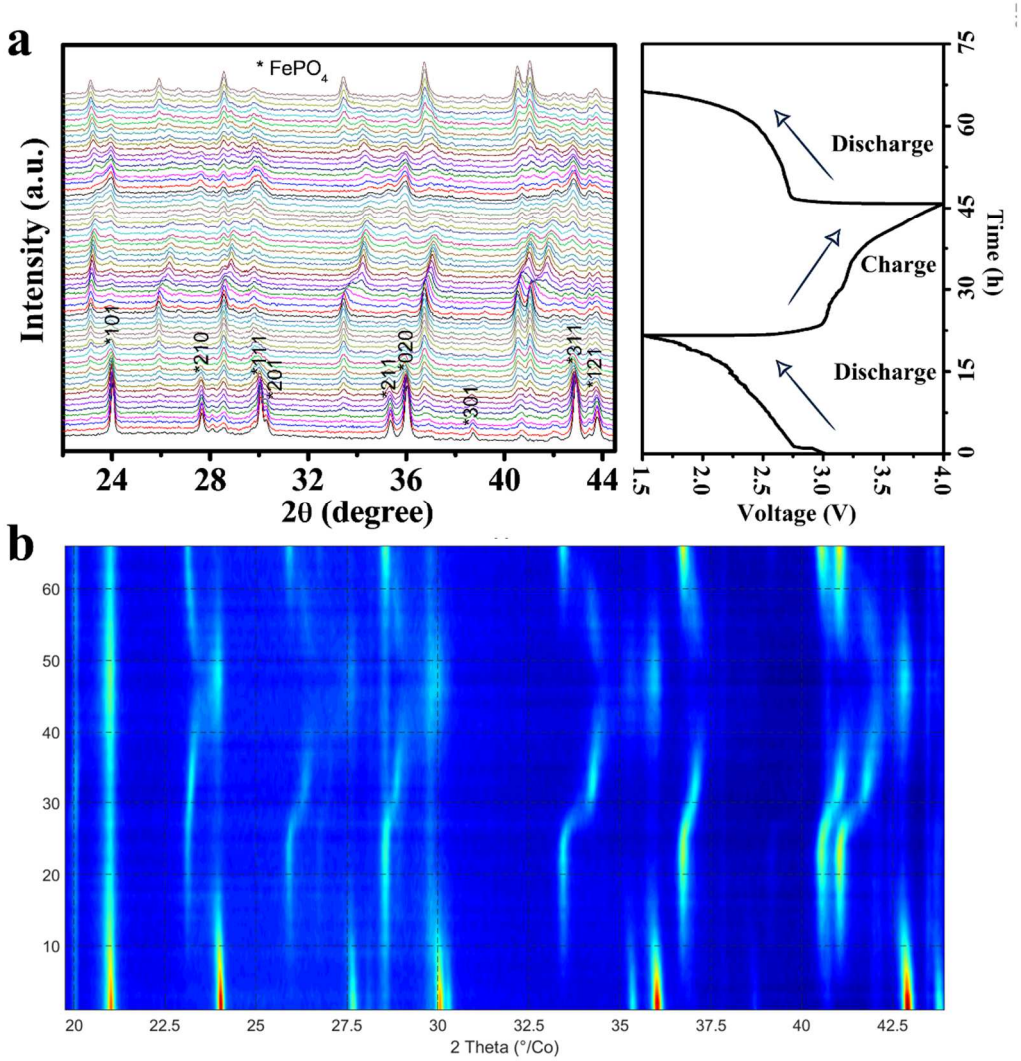

Figure 7: (a) *Operando* XRD analysis (Co Kα radiation) of FP@C vs. Na at C/10 during galvanostatic cycling. (b) Contour plot of the *operando* XRD results. The non-indexed peaks are due to *in situ* cell window.

3.4 Full cell performance

Lead is usually not considered as a possible anode for ion battery applications due to its weight and toxicity. Nevertheless, thanks to its extensive use in lead-acid batteries, its rate of recycling exceeds 99%, one of the highest on Earth in terms of recycling rates and sustainability [60]. Recently, the electrochemical properties of lead as negative electrode for SIB have been highlighted. [44,61,62] Lead shows an excellent capacity retention of 464 mAh/g after 50 cycles with a capacity loss of only 1.5% in 1 M $NaPF_6$/diglyme electrolytes, associating to a volumetric capacity of 5289 mAh/cm^3, as well as very interesting high rate performance with current densities up to ~2 A/g (cf. Figure S7 for more information about the electrochemical behaviour of Pb in half cell vs. Na).

The promising properties of lead anodes prompted us to propose a SIB full cell device with FP@C as the positive electrode and $Na_{15}Pb_4$ (prepared by electrochemical sodiation of Pb metal) as the negative electrode with a $NaPF_6$-diglyme electrolyte. Cell scheme, voltage profile and cycling properties of the FP@C/$Na_{15}Pb_4$ full cell are shown in Figure 8. The mass balance of anode and cathode was estimated based on the reversible capacity of the two electrodes, which is about 100 and 480 mAh/g at C/10 for cathode and anode, respectively. The full cell with FP@C cathode and $Na_{15}Pb_4$ anode has a mass loading of 5.6 and 1.1 mg, respectively, with a slight excess of the $Na_{15}Pb_4$ anode in order to counter the irreversible loss of Na^+ during the first discharge because of SEI formation and irreversible Na^+ trapping in $FePO_4$.

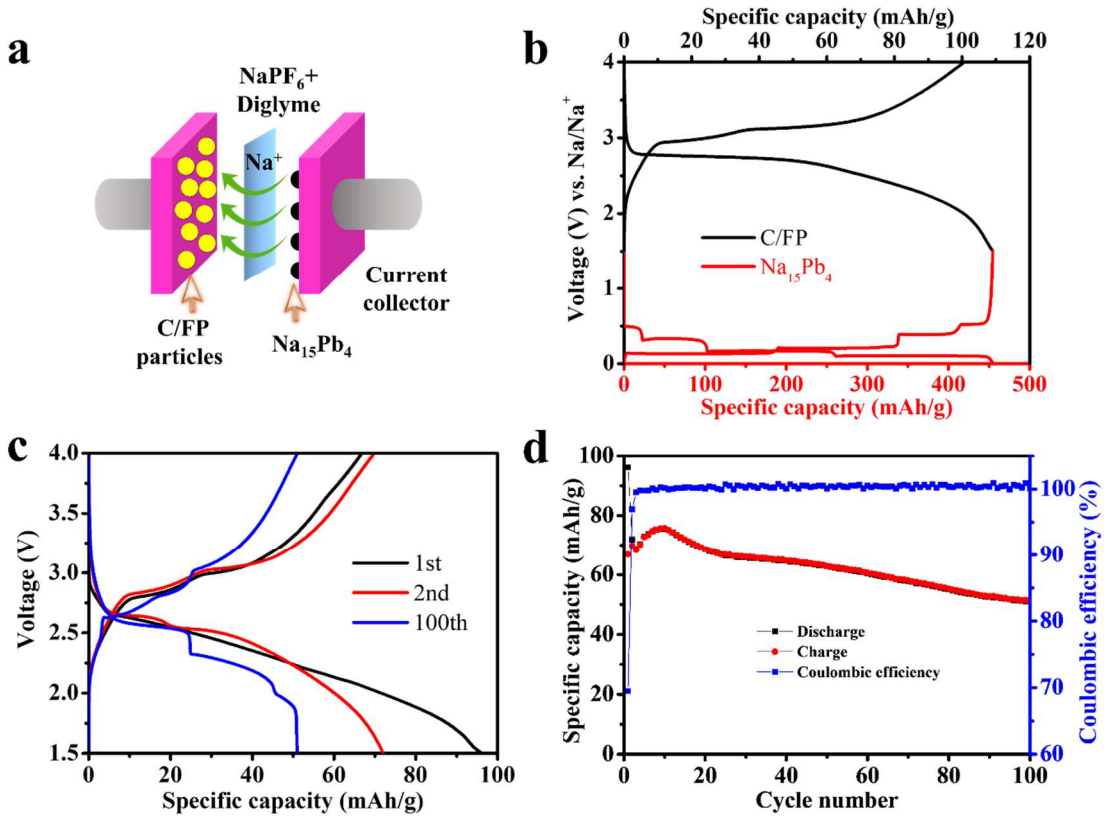

Figure 8: (a) Scheme of the FP@C/$Na_{15}Pb_4$ full cell. (b) Galvanostatic charge/discharge curves of the FP@C cathode (black) and the $Na_{15}Pb_4$ anode (red) in the voltage ranges 1.5-4 V and 0-1.5 V vs. Na^+/Na, respectively. (c-d) Capacity retention, coulombic efficiency and charge-discharge signatures of the FP@C/$Na_{15}Pb_4$ full cell at C/l0.

The initial discharge and charge specific capacities of the full cell are 96 and 67 mAh/g, correspondingly, with an initial coulombic efficiency of 70 %. Even though this corresponds to a relatively large irreversible capacity loss of about 30 % after the first cycle, the coulombic efficiency increases rapidly during the subsequent cycles, approaching 100 %. At the same time, the capacity decreases only slowly, stabilising at about 50 mAh/g, with 76% capacity retention even after 100 cycles.

4. Conclusions

A core-shell FP@C electrode fabricated by a very simple chemical process starting from commercial LFP@C materials displays correct preliminary rate performance and cycling stability vs. Na^+/Na, with a reversible capacity of 103 mAh/g, associating to 76 % of its theoretical capacity at C/20. A reversible discharge capacity of 60 mAh/g is also maintained

for more than a thousand cycles at the high rate of 2C. The carbon coating and the resulting composite electrode are responsible of this excellent battery performance. This kind of cathode material can be seen as a way to recycle spent LFP cathodes from LIBs.

FP@C provides excellent performance in full cell configuration vs. $Na_{15}Pb_4$, with a first discharge capacity of 96 mAh/g at C/10 and good cycle life with a 76 % capacity retention after 100 cycles. These first results on this innovating system provide an excellent starting point for the development of commercial Na-ion batteries for large-scale energy storage applications starting from LFP recycled from spent LIBs and a highly recyclable Pb-based anode material.

Acknowledgements

Financial support from the SATT AxLR Occitanie Méditerranée (Montpellier, France) through the project PLOBANA (AAP Pré-Maturation 2018, 2018-003451) as well as from the French National Research Agency (Labex STORE-EX, ANR-10-LABX-76-01) is gratefully acknowledged.

Conflicts of interest

The authors have no conflict of interest to declare.

References

[1] H. Pan, Y.-S. Hu, L. Chen, Room-temperature stationary sodium-ion batteries for large-scale electric energy storage, Energy Environ. Sci. 6 (2013) 2338–2360. doi:10.1039/c3ee40847g.

[2] B.L. Ellis, L.F. Nazar, Sodium and sodium-ion energy storage batteries, Curr. Opin. Solid State Mater. Sci. 16 (2012) 168–177. doi:10.1016/j.cossms.2012.04.002.

[3] V. Palomares, P. Serras, I. Villaluenga, K.B. Hueso, J. Carretero-González, T. Rojo, Na-ion batteries, recent advances and present challenges to become low cost energy storage systems, Energy Environ. Sci. 5 (2012) 5884–5901. doi:10.1039/c2ee02781j.

[4] D. Larcher, J.-M. Tarascon, Towards greener and more sustainable batteries for

electrical energy storage, Nat. Chem. 7 (2014) 19–29. doi:10.1038/nchem.2085.

[5] L. Monconduit, L. Croguennec, Na-ion Batteries, ISTE & John Wiley and Sons, London, New York, 2021.

[6] A. Ponrouch, M.R. Palacín, On the high and low temperature performances of Na-ion batteries: Hard carbon a case study, Electrochem. Commun. 54 (2015) 51–54. doi:10.1016/j.elecom.2015.03.002.

[7] S.P. Ong, V.L. Chevrier, G. Hautier, A. Jain, C. Moore, S. Kim, X. Ma, G. Ceder, Voltage, stability and diffusion barrier differences between sodium-ion and lithium-ion intercalation materials, Energy Environ. Sci. 4 (2011) 3680–3688. doi:10.1039/c1ee01782a.

[8] M.D. Slater, D. Kim, E. Lee, C.S. Johnson, Sodium-Ion Batteries, Adv. Funct. Mater. 23 (2012) 947–958. doi:10.1002/adfm.201200691.

[9] N. Tapia-Ruiz, A.R. Armstrong, H. Alptekin, M.A. Amores, H. Au, J. Barker, R. Boston, W.R. Brant, J.M. Brittain, Y. Chen, M. Chhowalla, Y. Choi, S.I.R. Costa, M. Crespo Ribadeneyra, S.A. Cussen, E.J. Cussen, W.I.F. David, A. V. Desai, S.A.M. Dickson, E.I. Eweka, J.D. Forero-Saboya, C.P. Grey, J.M. Griffin, P. Gross, X. Hua, J.T.S. Irvine, P. Johansson, M.O. Jones, M. Karlsmo, E. Kendrick, E. Kim, O. V. Kolosov, Z. Li, S.F.L. Mertens, R. Mogensen, L. Monconduit, R.E. Morris, A.J. Naylor, S. Nikman, C.A. O'Keefe, D.M.C. Ould, R.G. Palgrave, P. Poizot, A. Ponrouch, S. Renault, E.M. Reynolds, A. Rudola, R. Sayers, D.O. Scanlon, S. Sen, V.R. Seymour, B. Silván, M.T. Sougrati, L. Stievano, G.S. Stone, C.I. Thomas, M. Titirici, J. Tong, T.J. Wood, D.S. Wright, R. Younesi, 2021 roadmap for sodium-ion batteries, J. Phys. Energy. 3 (2021) 031503. doi:10.1088/2515-7655/ac01ef.

[10] B. Pandit, S.R. Rondiya, N.Y. Dzade, S.F. Shaikh, N. Kumar, E.S. Goda, A.A. Al-Kahtani, R.S. Mane, S. Mathur, R.R. Salunkhe, High Stability and Long Cycle Life of Rechargeable Sodium-Ion Battery Using Manganese Oxide Cathode: A Combined Density Functional Theory (DFT) and Experimental Study, ACS Appl. Mater. Interfaces. 13 (2021) 11433–11441. doi:10.1021/acsami.0c21081.

[11] H. Su, S. Jaffer, H. Yu, Transition metal oxides for sodium-ion batteries, Energy Storage Mater. 5 (2016) 116–131. doi:10.1016/j.ensm.2016.06.005.

[12] X. Deng, Z. Chen, Y. Cao, Transition metal oxides based on conversion reaction for sodium-ion battery anodes, Mater. Today Chem. 9 (2018) 114–132. doi:10.1016/j.mtchem.2018.06.002.

[13] Q. Liu, Z. Hu, M. Chen, C. Zou, H. Jin, S. Wang, S. Chou, S. Dou, Recent Progress of Layered Transition Metal Oxide Cathodes for Sodium-Ion Batteries, Small. 15 (2019) 1805381. doi:10.1002/smll.201805381.

[14] Y. Zhang, Y. Pei, W. Liu, S. Zhang, J. Xie, J. Xia, S. Nie, L. Liu, X. Wang, AlPO4-coated P2-type hexagonal Na0.7MnO2.05 as high stability cathode for sodium ion battery, Chem. Eng. J. 382 (2020) 122697. doi:10.1016/j.cej.2019.122697.

[15] Y. Zhang, Y. Ouyang, L. Liu, J. Xia, S. Nie, W. Liu, X. Wang, Synthesis and characterization of Na0.44MnO2 nanorods/graphene composite as cathode materials for sodium-ion batteries, J. Cent. South Univ. 26 (2019) 1510–1520. doi:10.1007/s11771-019-4107-6.

[16] Q. Cheng, X. Zhao, G. Yang, L. Mao, F. Liao, L. Chen, P. He, D. Pan, S. Chen, Recent advances of metal phosphates-based electrodes for high-performance metal ion batteries, Energy Storage Mater. 41 (2021) 842–882. doi:10.1016/j.ensm.2021.07.017.

[17] Y. Fang, J. Zhang, L. Xiao, X. Ai, Y. Cao, H. Yang, Phosphate Framework Electrode Materials for Sodium Ion Batteries, Adv. Sci. 4 (2017) 1600392. doi:10.1002/advs.201600392.

[18] G. Chen, Q. Huang, T. Wu, L. Lu, Polyanion Sodium Vanadium Phosphate for Next Generation of Sodium-Ion Batteries—A Review, Adv. Funct. Mater. 30 (2020) 1–23. doi:10.1002/adfm.202001289.

[19] C.D. Wessells, Batteries Containing Prussian Blue Analogue Electrodes, in: L. Monconduit, L. Croguennec (Eds.), Na-ion Batter., Wiley, London, New York, 2021: pp. 265–311. doi:10.1002/9781119818069.ch7.

[20] J. Chen, L. Wei, A. Mahmood, Z. Pei, Z. Zhou, X. Chen, Y. Chen, Prussian blue, its analogues and their derived materials for electrochemical energy storage and conversion, Energy Storage Mater. 25 (2019) 585–612. doi:10.1016/j.ensm.2019.09.024.

[21] M.T. Sougrati, A. Darwiche, X. Liu, A. Mahmoud, R.P. Hermann, S. Jouen, L. Monconduit, R. Dronskowski, L. Stievano, Batteries Transition-Metal Carbodiimides as Molecular Negative Electrode Materials for Lithium- and Sodium-Ion Batteries with Excellent Cycling Properties, Angew. Chem. Int. Ed. 55 (2016) 5090–5095. doi:10.1002/anie.201600098.

[22] M.T. Sougrati, J.J. Arayamparambil, X. Liu, M. Mann, A. Slabon, L. Stievano, R. Dronskowski, Carbodiimides as energy materials: which directions for a reasonable future?, Dalt. Trans. 47 (2018) 10827–10832. doi:10.1039/C8DT01846D.

[23] K. Song, C. Liu, L. Mi, S. Chou, W. Chen, C. Shen, Recent Progress on the Alloy-Based Anode for Sodium-Ion Batteries and Potassium-Ion Batteries, Small. 17 (2021) 1903194. doi:10.1002/smll.201903194.

[24] H. Liu, X.-B. Cheng, J.-Q. Huang, S. Kaskel, S. Chou, H.S. Park, Q. Zhang, Alloy Anodes for Rechargeable Alkali-Metal Batteries: Progress and Challenge, ACS Mater. Lett. 1 (2019) 217–229. doi:10.1021/acsmaterialslett.9b00118.

[25] M. Lao, Y. Zhang, W. Luo, Q. Yan, W. Sun, S.X. Dou, Alloy-Based Anode Materials toward Advanced Sodium-Ion Batteries, Adv. Mater. 29 (2017) 1700622. doi:10.1002/adma.201700622.

[26] W. Luo, F. Shen, C. Bommier, H. Zhu, X. Ji, L. Hu, Na-Ion Battery Anodes: Materials and Electrochemistry., Acc. Chem. Res. 49 (2016) 231–240. doi:10.1021/acs.accounts.5b00482.

[27] E. Irisarri, A. Ponrouch, M.R. Palacin, Review—Hard Carbon Negative Electrode Materials for Sodium-Ion Batteries, J. Electrochem. Soc. 162 (2015) A2476–A2482. doi:10.1149/2.0091514jes.

[28] H. Hou, X. Qiu, W. Wei, Y. Zhang, X. Ji, Carbon Anode Materials for Advanced Sodium-Ion Batteries, Adv. Energy Mater. 7 (2017) 1602898. doi:10.1002/aenm.201602898.

[29] Y. You, A. Manthiram, Progress in High-Voltage Cathode Materials for Rechargeable Sodium-Ion Batteries, Adv. Energy Mater. 8 (2018) 1701785. doi:10.1002/aenm.201701785.

[30] P. Moreau, D. Guyomard, J. Gaubicher, F. Boucher, Structure and Stability of Sodium Intercalated Phases in Olivine FePO4, Chem. Mater. 22 (2010) 4126–4128. doi:10.1021/cm101377h.

[31] A. Saracibar, J. Carrasco, D. Saurel, M. Galceran, B. Acebedo, H. Anne, M. Lepoitevin, T. Rojo, M. Casas-Cabanas, Investigation of sodium insertion-extraction in olivine NaxFePO4 ($0 \leq x \leq 1$) using first-principles calculations., Phys. Chem. Chem. Phys. 18 (2016) 13045–13051. doi:10.1039/c6cp00762g.

[32] D. Saurel, M. Galceran, M. Reynaud, H. Anne, M. Casas-Cabanas, Rate dependence of the reaction mechanism in olivine NaFePO4 Na-ion cathode material, Int. J. Energy Res. 42 (2018) 3258–3265. doi:10.1002/er.4078.

[33] D. Saurel, A. Pendashteh, M. Jáuregui, M. Reynaud, M. Fehse, M. Galceran, M. Casas-Cabanas, Experimental Considerations for Operando Metal-Ion Battery Monitoring using X-ray Techniques, Chem. Methods. 1 (2021) 249–260. doi:10.1002/cmtd.202100009.

[34] P. Barpanda, G. Oyama, S. Nishimura, S.-C. Chung, A. Yamada, A 3.8-V earth-abundant sodium battery electrode, Nat. Commun. 5 (2014). doi:10.1038/ncomms5358.

[35] Y. Fang, Z. Chen, L. Xiao, X. Ai, Y. Cao, H. Yang, Recent Progress in Iron-Based Electrode Materials for Grid-Scale Sodium-Ion Batteries, Small. 14 (2018) 1703116. doi:10.1002/smll.201703116.

[36] J. Lu, S.C. Chung, S. Nishimura, A. Yamada, Phase Diagram of Olivine NaxFePO4 ($0 < x < 1$), Chem. Mater. 25 (2013) 4557–4565. doi:10.1021/cm402617b.

[37] K. Walczak, A. Kulka, B. Gędziorowski, M. Gajewska, J. Molenda, Surface investigation of chemically delithiatied FePO4 as a cathode material for sodium ion batteries, Solid State Ionics. 319 (2018) 186–193. doi:10.1016/j.ssi.2018.01.041.

[38] Y. Zhu, Y. Xu, Y. Liu, C. Luo, C. Wang, Comparison of electrochemical performances of olivine NaFePO4 in sodium-ion batteries and olivine LiFePO4 in lithium-ion batteries, Nanoscale. 5 (2013) 780–787. doi:10.1039/C2NR32758A.

[39] M. Dixit, H. Engel, R. Eitan, D. Aurbach, M.D. Levi, M. Kosa, D.T. Major, Classical and Quantum Modeling of Li and Na Diffusion in FePO4, J. Phys. Chem. C. 119 (2015) 15801–15809. doi:10.1021/acs.jpcc.5b00405.

[40] Q. Fan, L. Lei, G. Yin, Y. Chen, Y. Sun, Direct growth of FePO4/graphene hybrids for Li-ion and Na-ion storage, Electrochem. Commun. 38 (2014) 120–123. doi:10.1016/j.elecom.2013.11.006.

[41] Y. Liu, Y. Xu, X. Han, C. Pellegrinelli, Y. Zhu, H. Zhu, J. Wan, A.C. Chung, O. Vaaland, C. Wang, L. Hu, Porous Amorphous FePO4 Nanoparticles Connected by Single-Wall Carbon Nanotubes for Sodium Ion Battery Cathodes, Nano Lett. 12 (2012) 5664–5668. doi:10.1021/nl302819f.

[42] Y. Fang, L. Xiao, J. Qian, X. Ai, H. Yang, Y. Cao, Mesoporous Amorphous FePO4 Nanospheres as High-Performance Cathode Material for Sodium-Ion Batteries., Nano

Lett. 14 (2014) 3539–3543. doi:10.1021/nl501152f.

[43] L.D. Ellis, B.N. Wilkes, T.D. Hatchard, M.N. Obrovac, In Situ XRD Study of Silicon, Lead and Bismuth Negative Electrodes in Nonaqueous Sodium Cells, J. Electrochem. Soc. 161 (2014) A416–A421. doi:10.1149/2.080403jes.

[44] A. Darwiche, R. Dugas, B. Fraisse, L. Monconduit, Reinstating lead for high-loaded efficient negative electrode for rechargeable sodium-ion battery, J. Power Sources. 304 (2016) 1–8. doi:10.1016/j.jpowsour.2015.10.087.

[45] M. Galceran, A. Guerfi, M. Armand, K. Zaghib, M. Casas-Cabanas, The Critical Role of Carbon in the Chemical Delithiation Kinetics of LiFePO4, J. Electrochem. Soc. 167 (2020) 070538. doi:10.1149/1945-7111/ab7ce3.

[46] G. Grosse, PC-Mos II, Version 1.0 Manual and Program Documentation, (1993).

[47] A. Darwiche, R. Dugas, B. Fraisse, L. Monconduit, Reinstating lead for high-loaded efficient negative electrode for rechargeable sodium-ion battery, J. Power Sources. 304 (2016) 1–8. doi:10.1016/j.jpowsour.2015.10.087.

[48] M. Morcrette, Y. Chabre, G.B.M. Vaughan, G.G. Amatucci, J.-B. Leriche, S. Patoux, C. Masquelier, J.-M. Tarascon, In situ X-ray diffraction techniques as a powerful tool to study battery electrode materials, Electrochim. Acta. 47 (2002) 3137–3149. doi:10.1016/S0013-4686(02)00233-5.

[49] M. Galceran, D. Saurel, B. Acebedo, V. V. Roddatis, E. Martin, T. Rojo, M. Casas-Cabanas, The mechanism of NaFePO4 (de)sodiation determined by in situ X-ray diffraction., Phys. Chem. Chem. Phys. 16 (2014) 8837–8842. doi:10.1039/c4cp01089b.

[50] C.M. Burba, R. Frech, Raman and FTIR Spectroscopic Study of Li[sub x]FePO[sub 4] (0≤x≤1), J. Electrochem. Soc. 151 (2004) A1032–A1038. doi:10.1149/1.1756885.

[51] C.M. Burba, R. Frech, Vibrational spectroscopic investigation of structurally-related LiFePO4, NaFePO4, and FePO4 compounds, Spectrochim. Acta A Mol. Biomol. Spectrosc. 65 (2006) 44–50. doi:10.1016/j.saa.2005.09.025.

[52] S. Reich, C. Thomsen, Raman spectroscopy of graphite., Philos. Trans. A Math. Phys. Eng. Sci. 362 (2004) 2271–2288. doi:10.1098/rsta.2004.1454.

[53] Y. Wang, M.-Q. Wang, L.-L. Lei, Z.-Y. Chen, Y.-S. Liu, S.-J. Bao, FePO4 embedded in nanofibers consisting of amorphous carbon and reduced graphene oxide as an enzyme mimetic for monitoring superoxide anions released by living cells, Microchim. Acta. 185 (2018) 140. doi:10.1007/s00604-018-2691-z.

[54] R. Dedryvère, M. Maccario, L. Croguennec, F. Le Cras, C. Delmas, D. Gonbeau, X-ray photoelectron spectroscopy investigations of carbon-coated Li xFePO4 materials, Chem. Mater. 20 (2008) 7164–7170. doi:10.1021/cm801995p.

[55] R. Amisse, M.T. Sougrati, L. Stievano, C. Davoisne, G. Dražić, B. Budic, R. Dominko, C. Masquelier, Singular structural and electrochemical properties in highly defective “LiFePO4” powders, Chem. Mater. 27 (2015) 4261–4273. doi:10.1021/acs.chemmater.5b00470.

[56] Y. Liu, S. Xu, S. Zhang, J. ZHang, J. Fan, Y. Zhou, Direct growth of FePO4/reduced graphene oxide nanosheet composite for sodium-ion battery, J. Mater. Chem. A. 3

(2015) 5501–5508. doi:10.1039/C5TA00199D.

[57] C. Heubner, S. Heiden, B. Matthey, M. Schneider, A. Michaelis, Sodiation vs. Lithiation of FePO4: A comparative kinetic study, Electrochim. Acta. 216 (2016) 412–419. doi:10.1016/j.electacta.2016.09.041.

[58] Z. Zhang, Y. Du, Q. Wang, J. Xu, Y. Zhou, J. Bao, J. Shen, X. Zhou, A Yolk–Shell-Structured FePO 4 Cathode for High-Rate and Long-Cycling Sodium-Ion Batteries, Angew. Chemie Int. Ed. 59 (2020) 17504–17510. doi:10.1002/anie.202008318.

[59] K. Tang, X. Yu, J. Sun, H. Li, X. Huang, Kinetic analysis on LiFePO4 thin films by CV, GITT, and EIS, Electrochim. Acta. 56 (2011) 4869–4875. doi:10.1016/j.electacta.2011.02.119.

[60] X. Tian, Y. Wu, P. Hou, S. Liang, S. Qu, M. Xu, T. Zuo, Environmental impact and economic assessment of secondary lead production: Comparison of main spent lead-acid battery recycling processes in China, J. Clean. Prod. 144 (2017) 142–148. doi:10.1016/j.jclepro.2016.12.171.

[61] C. Kim, H. Kim, M.K. Sadan, M. Jeon, G.-B. Cho, T.-H. Nam, K.-K. Cho, J.-H. Ahn, H.-J. Ahn, A high rate and long-cycle-life anode based on micrometer-sized Pb powder for sodium-ion batteries, J. Alloys Compd. 886 (2021) 161240. doi:10.1016/j.jallcom.2021.161240.

[62] V. Ahuja, S. Singh, R. Vengarathody, P. Senguttuvan, Room-Temperature Synthesis and Stable Na-Ion Storage Performance of Two-Dimensional Mixed Lead-Bismuth Oxychloride Heterostructure, ECS Meet. Abstr. MA2021-01 (2021) 254–254. doi:10.1149/MA2021-014254mtgabs.